ACS OMEGA

http://pubs.acs.org/journal/acsodf

Article

Thiophene-Appended Benzothiazole Compounds for Ratiometric Detection of Copper and Cadmium Ions with Comparative Density Functional Theory Studies and Their Application in Real-Time Samples

Palani Purushothaman and Subramanian Karpagam*

Cite This: *ACS Omega* 2022, 7, 41361−41369

Read Online

ACCESS | Metrics & More | Article Recommendations | Supporting Information

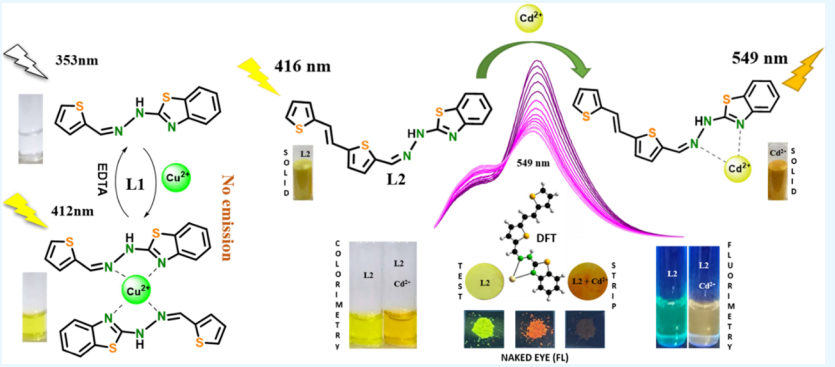

ABSTRACT: A thirst for the development of a simple fluorescence probe for enhanced sensing application has been achieved by synthesizing a stupendous thiophene-appended benzothiazole-conjugated compound **L2**. The synthesized compound **L2** was characterized using nuclear magnetic resonance and mass spectrometry techniques. Furthermore, a photophysical property of **L1** and **L2** reveals the enhanced emission spectrum of **L2** because of a restricted spin−orbital coupling as a result of increased conjugation compared to the ligand **L1**. Therefore, comparative studies were undertaken for **L1** and **L2**. Henceforth, **L2** was deployed for the ratiometric detection of Cd^{2+} ions in THF:water and **L1** for the detection of Cu^{2+} ions in THF medium. The chemosensor **L2** shows an outstanding water tolerance up to 60% and is stable between pH 2 and 7. This level of water tolerance and stability make **L2** a suitable probe for analyzing real-time and biological samples. While the cadmium ion was added to **L2**, there was a significant red shift in emission from 496 to 549 nm, which indicates the controlled ICT due to complex formation. The metal−ligand complexation was also confirmed by noticing a decreased band gap of metal complex compared to the ligand as calculated using Tauc's plot with solid-phase UV data. The stoichiometric ratio was obtained by Job's plot that exhibited a 1:1 ratio of **L2** and Cd^{2+} ions, and the limit of detection (LOD) was found to be 2.25 nM by the photoluminescence spectroscopic technique. The fluorescence lifetime of both **L2** and **L2**-Cd^{2+} was found to be 58.3 ps and 0.147 ns, respectively. Alongside, the colorimetric-assisted ratiometric detection of Cu^{2+} by **L1** with 1:2 stoichiometric ratio having an LOD of 1.06×10^{-7} M was also performed. Furthermore, the practical applicability of the probe **L2** in sensing cadmium was tested in sewage water and vegetable extract; the recovery was approximately 98 and 99%, respectively. The experimental data were supported by theoretical investigation of structures of **L1**, **L2**, **L1**-Cu^{2+}, and **L2**-Cd^{2+}, complex formation, charge transfer mechanism, and band gap measurements done by quantum chemical density functional theory calculations.

1. INTRODUCTION

A struggle for the substantial discovery of scintillating fluorescent compounds for sensing application has been a constant search for a long period of time. A simple alteration to already-existing compounds and reaction procedures will lead to a subtle way for the development of enhanced fluorescent probes for sensing toxic and harmful chemicals, which were discarded into the ecosystem because of an anthropogenic factor. Among many other sensing techniques, fluorescence (FL)-based sensing probes have exceptional sensitivity, selectivity, an easier operating procedure, a wide pH range, and capability to deal

Received: August 11, 2022
Accepted: October 20, 2022
Published: November 2, 2022

with real-time sample analysis.[1−5] In such a context, thiophene has been proven to be an excellent moiety as a precursor for the development of various sensing probes because of its structural and synthetic diversity, color tuning of the absorption and emission spectra, optimized band gap, and charge transfer ability. Despite all such useful properties, the fluorescent quantum yield of thiophene compounds is very low because of strong spin−orbit coupling of sulfur. This ultimately results in efficient intersystem crossing (ISC) coupled with a nonradiative process.[6]

However, the shortcomings can be rectified by increasing the conjugation length, and the corresponding fluorescent quantum yield (Φ_F) thus increases. Keeping this in mind, a novel fluorescent probe **L2** has been synthesized by having **L1** as reference. The **L1** compound was reported earlier by Lindgren et al.[7] However, **L1** lacks fluorescent emission because of a strong ISC and nonradiative emission between T_1 (triplet excited state) and S_0 (singlet ground state). Henceforth, the synthesis, properties, spectral data, and application of both **L1** and **L2** (Figure 1) were compared and presented.

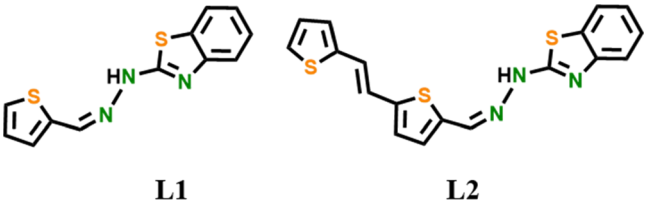

Figure 1. Structure of the synthesized probes **L1** and **L2**.

In effect to sensing application, we employed both the compounds for various selectivity processes and found that both **L1** and **L2** were good at metal ion detection in an experimentally calculated concentration and also in real-time samples.[8] The detection of metal ions is a crucial part because it made to the alarming level of contamination in the ecosystem. Obviously, a modernization and ostentatious living crippled with time-consuming durables for an outstanding result brought in an enormous industrialization, which uses harmful chemicals and minerals. These industries release toxic metal ions and other toxic organic molecules into the environment.[9−11] Among many metal ions, cadmium and copper are the two heavy metals that had been detected by the ligands **L1** and **L2**, respectively. The investigation by UV−vis and photoluminescence (PL) studies displayed an outstanding selectivity toward Cu^{2+} and Cd^{2+} by the ligands.

Several compounds in the reported literature were considering just a single wavelength either quenched or enhanced.[12−15] To the best of the author's knowledge, **L2** is the first compound of its kind of simple conjugated thiophene-appended benzothiazole moiety for the ratiometric detection of metal ions.[16,17] Because ratiometric detection simultaneously measures the ratio of two emission bands,[18,19] it can exclude the distortion from the external environment and produce results that are more pronounced than intensity-based measurement.

Henceforth, we report a novel fluorescent probe **L2** that contains a conjugated thiophene unit as the fluorophore and benzothiazole as the recognition unit for the ratiometric detection of Cd^{2+}. The expected fluorescent enhancement and red shift happen after the addition of metal to the probe. The charge transfer between **L2** and Cd^{2+} after complexation was found to be the sole responsible factor for the FL change. We also provide comparative spectral data of ligands **L1** and **L2**. At the end, we presented the density functional theory (DFT) studies of the synthesized ligand and complex.[20−22] The comparative outcome of **L1** and **L2** from our results are presented in the table below (Table 1).

Table 1. Comparative Outcome of Ligands L1 and L2

properties and outcomes	L1	L2
synthesis	single step	three steps
optical activity	UV active	UV and FL active
metal ion sensed	Cu^{2+}	Cd^{2+}
method of sensing	ratiometric	ratiometric
technique	UV	fluorescence
solvent used	THF	THF:water
AIEE	NIL	60%
$\Lambda_{max(abs)}$	353 nm	412 nm
$\Lambda_{max(emi)}$	NIL	496 nm
isosbestic point	383 nm	523 nm
ratiometric plot	A_{353}/A_{412}	F_{552nm}/F_{496nm}
$n-\pi^*$ transition	412 nm	552 nm
ligand−metal ratio	2:1	1:1
binding constant	5.93×10^{-3} M^{-1}	1.2×10^{-2} M^{-1}
charge transfer mechanism	metal-mediated ICT	MLCT
band gap (L)	2.83 eV	2.31 eV
band gap (complex)	2.01 eV	2.24 eV
LOD	1.06×10^{-7} M	2.25×10^{-9} M

2. EXPERIMENTAL PROCEDURES

2.1. Materials and Methods. 2-Thiophene carboxaldehyde, 2-hydrazino benzothiazole, and all other chemicals were purchased from Sigma-Aldrich. All the solvents used for synthesis, extraction, and analytical techniques were of analytical standard and used without any further purification.

2.2. General Physical Measurements. FT-IR spectra were obtained using KBr discs with a Shimadzu FT-IR spectrometer (400−4000 cm^{-1}). The NMR spectra were recorded on a Bruker (400 MHz) spectrometer, and chemical shifts were reported in δ (ppm). High-resolution mass spectrometry (HRMS) spectra were recorded on a WATER-XEVO G2XS-QT. Absorption spectra were recorded using an Agilent 8453 UV−visible diode array spectrophotometer using THF solvent. An Edinburg FLS 980 spectrometer was used to perform the steady-state photoluminescence studies. Life time determination of FL was carried out in JOBIN-VYON M/S. The experiment was carried out in a 405 nm LED for the proximal excitation of sample having actual excitation pulse at 416 nm. Ludox (Colloidal silica) was used as a prompt while measuring life time.

2.3. Sample Preparation. The concentration of the ligand **L1**, **L2** stock solution was 1×10^{-4} M in THF, and the Na^+, K^+, Ag+, Ca^{2+}, Mg^{2+}, Zn^{2+}, Cu^{2+}, Cu^+, Zr^{2+}, Fe^{2+}, Hg^{2+}, Co^{2+}, Ni^{2+}, Cd^{2+}, and Mn^{2+} metal ion stock solution (1×10^{-2} M) was prepared in double distilled water. The stock solutions of ligands **L1** and **L2** of 10^{-4} M were prepared using THF and HEPES aqueous solution (pH 6.5−7.5) in the ratio 2:3 and 1:0, respectively. All other optical spectral characterization studies were performed with the above prepared stock solutions.

2.4. Computational Details. DFT calculations of ligands **L1** and **L2** and their respective Cu^{2+} and Cd^{2+} complexes were completely optimized by using the G16 package. The B3LYP functional was combined with the 6-31G** basis set to optimize

https://doi.org/10.1021/acsomega.2c05157
ACS Omega 2022, 7, 41361−41369

hydrogen, carbon, nitrogen, and oxygen atoms and 6-31G(d)/LANL2DZ for Cu^{2+} and Cd^{2+}. Frontier molecular structures and electronic geometries were obtained from the Gauss view 6.1.1 molecular visualization program.

2.5. Real-Time Sample Analysis. The vegetable extract was obtained by simply blending the sprouted potato in a mixer and was filtered using a Whatman filter paper to remove the insoluble junks. Furthermore, the extract's pH was adjusted to the optimized working range between 6.5 and 7.5. The sewage water was collected and filtered to remove the insoluble particle, and the sensing application was proceeded after spiking up the solution with a metal ion of 10^{-2} M concentration. The obtained solution was used for photoluminescence studies.

2.6. Synthesis of Precursors and Chemosensor and Its Characterization. *2.6.1. Synthesis of (E)-5-(2-(Thiophen-2-yl)vinyl)thiophene-2-carbaldehyde (**P2**).* The compound (*E*)-1,2-bis(2-thenyl)ethylene (**P1**) obtained by McMurry coupling as reported by Mahesh et al.,[23] and then **P1** was further used for synthesizing (*E*)-5-(2-(thiophen-2-yl)vinyl)thiophene-2-carbaldehyde (**P2**). 73.3 mmol DMF was slowly added to **P1** (13 mmol) in DCE at 0 °C. Then phosphorous trichloride (58.5 mmol) was added to the above mixture under a nitrogen atmosphere. The reaction mixture was then stirred at room temperature overnight to obtained monoaldehyde as a major product. The resulting suspension was cooled, diluted with cold water, and neutralized with sodium carbonate. The obtained crude product was extracted with DCM and dried. The resulting orange red crude product was purified with column chromatography using hexane and ethyl acetate as an eluent. Thin-layer chromatography observation shows two spots: first, a bright yellow fluorescent and second, a vibrant sky-blue fluorescent. The two spots were collected separately at 1 and 3% eluents, respectively. A bright yellow fluorescent product was confirmed as P2. Yield: 73.65%, FT-IR: (KBR, ν/cm^{-1}): 1654.89(−C═O), 953.17 (*trans*-vinylene). ^{1}H ($CDCl_3$, 400 MHz, δ ppm): 10.113(1H, s), 7.919(1H, d), 7.558(2H, q), 7.418(1H, d), 7.384(1H, d), 7.311(2H, t), and the final confirmation was obtained from HRMS (ESI) data: calculated for $C_{11}H_8OS_2$ (M + H) 220.00, found 221.00 (Figure S1).

L1 was prepared as per the procedure mentioned in ref 7 for further spectral studies. **L2** was prepared by reacting P2 (0.2 g, 0.9 mmol) with 2-hydrazinobenzothiazole (0.149 g, 0.9 mmol) in ethanol, RT for 3 h (Scheme 1). The reaction was catalyzed by a few drops of concentrated sulfuric acid. A visible yellow to reddish orange change was observed when sulfuric acid was added to the reaction mixture. The final product was filtered with Whatman filter paper and washed thoroughly with methanol until the starting material was removed completely. Later, the compound was dried under vacuum for 2 h. The solid itself shows a bright yellowish orange fluorescent color (0.156 g, yield 83%) ^{1}H (DMSO, 400 MHz, δ ppm): 8.221 (1H, s), 7.750 (1H, d), 7.483 (1H, d), 7.397 (1H, d) 7.315 (3H, m), 7.227 (1H, s), 7.183 (1H, d), 7.140 (3H, m), the −NH proton was not observed in NMR because of fast H-exchange in the NMR times scale[24] (Figure S2a). However, we preliminarily confirmed the presence of NH protons by FT-IR, and the final confirmation was done with HRMS (ESI) data: calculated for $C_{18}H_{13}N_3S_3$ (M + H) 367.0360, found 368.0367 (Figure S2b). ^{13}C NMR (400 MHz, DMSO-d6): δ 167.07, 143.92, 142.00, 138.26, 131.26, 128.66, 128.11, 128.03, 126.64, 126.4, 123.20, 122.21 and 121.32 (Figure S2c).

Scheme 1. Representation of Reactions Involved in Synthesis of Desired Product L2

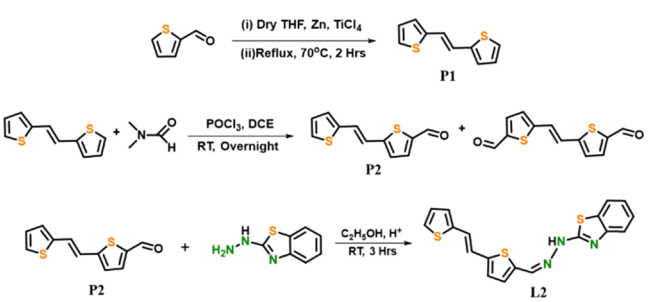

3. RESULTS AND DISCUSSION

3.1. Characterization and Optical Characteristics of L1 and L2. **L2** was completely characterized by FT-IR, NMR, and HRMS. The formation of products was confirmed by NMR and mass spectroscopy. The formation of an imine group was confirmed by the presence of a sharp singlet at 8.221 ppm (−CH═N), and a trans vinylene-linked thiophene was confirmed by the value of the corresponding coupling constant (J = 17.2 Hz) in ^{1}H NMR. The final confirmation was also done with HRMS, and experimental data (368.0367) were in good agreement with the calculated data (367.0360) for the **L2** compound ($C_{18}H_{13}N_3S_3$). The respective isotopic peaks were also obtained in a perfect ratio of mass 369.0361, 370.0322, and 371.0329.

The optical behavior of **L1** and **L2** was investigated by UV−vis and PL spectroscopic techniques. The synthesized thiophene-appended imine-linked thiazole moieties did not show a significant change in absorbance and emission intensity by the solvatochromic effect. However, both **L1** and **L2** have shown a significant red shift with highly polar DMSO and DMF. Thus, it can be concluded that high polarity has been required to relax the ICT excited state to result in red-shifted emission.

THF was a chosen as a solvent because the red shift of the ligand peak in UV−vis absorbance was almost closer to the one which was observed for the highly polar solvents. A point to note is that THF is also an easier solvent to handle than DMSO and DMF. Later, aggregation studies were performed in different ratios of water and THF. **L1** was found to be tolerant to just 10% of water, but **L2** shows a greater tolerance up to 60% of water. An aggregation-induced emission enhancement (AIEE) was seen until 60% of water. Later, the aggregation-induced quenching took place (Figure 2a). The pH study was also conducted in the

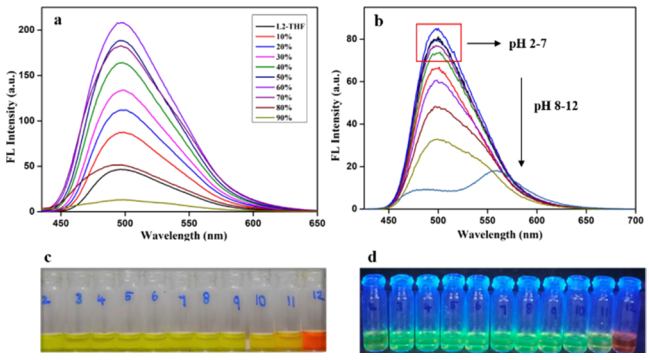

Figure 2. (a) Aggregation effect of **L2**. (b) Effect of pH on the emission spectrum of **L2**. (c) Visible color gradation of **L2** in THF with different pH solutions. (d) FL observance of the pH effect of **L2** in THF.

https://doi.org/10.1021/acsomega.2c05157
ACS Omega 2022, 7, 41361−41369

varying range of pH from 2 to 12. The FL intensity of **L2** in varying pH is given in Figure 2b,d. The naked eye observation clearly depicts a color change only in pH 10 to 12 in UV light Figure 2c and in pH 11−12 in FL illumination. However, the photoluminescence investigation shows a similar emission of **L2** in the pH range of 2−7; there was a significant decrease in pH from 8 to 12. In addition to that, there was no significant red shift in emission wavelength in either acidic or basic pH. Along with this, there was a significant quenching of FL of **L2** in pH 12. Thus, the optimized neutral pH of range 6.5−7.5 was chosen to proceed for further optical characterization and sensing applications. The quantum yield of **L2** by the relative method was found to be 0.002939. The procedure for calculating quantum yield has been presented at the end of the Supporting Information.

3.2. Sensing Behavior of Probes L1 and L2. The cation sensing capability of both the ligands was evaluated in THF and HEPES buffer solutions of ligand and metal solution, respectively. Based on the water tolerance studies, we prepared **L2** stock in THF and HEPES buffer in the ratio 2:3, whereas the **L1** was prepared in THF alone. The higher energy (weak band) absorption spectra of **L1** were observed at 230 and 274 nm, which was due to $\pi-\pi^*$ transition, and the lower energy (strong band) absorption spectra appeared at 353 nm which is responsible for the strong intramolecular charge transfer between the donor (thiophene) and acceptor (thiazole). Similarly, the weak and strong bands of **L2** were observed at 253, 320, and 416 nm. Also, **L2** displayed a strong emission spectrum at 496 nm (Figure S3).

The solid-phase absorbance spectra of both the ligand and its metal complex show a hypochromic shift (∼29 to 92 nm) and show a broad spectrum because of the disappearance of $\pi-\pi^*$ transition as a result of restricted C−C rotation (Figure S4).

An outstanding selectivity of **L1** toward Cu^{2+} had been seen through a naked eye. The instantaneous change from colorless to yellow was seen when Cu^{2+} was added to **L1** (Figure 3c). There was no significant change in color when other competitive metal ions were added to the ligand solution. This was confirmed by the UV−vis absorbance study. As shown in Figure 4a, it can be undoubtedly concluded that **L1** is highly selective to cupric ions. The detail regarding the noninterference of other metal ions toward Cu^{2+} sensing is displayed as a bar chart (Figure S5a). The abrupt decrease of absorbance at 353 nm (ICT of the ligand) and the emergence of a new peak at 412 nm ($n-\pi^*$) clearly show the metal complexation followed by metal-mediated ICT. Thus, **L1** proved to be a highly selective sensing probe for cupric ions. However, as mentioned earlier because of spin−orbit coupling the compound does not show emission under FL spectra. Hence, it restricts to be an excellent naked eye colorimetric sensor toward Cu^{2+} ions.

Desire of developing a fluorometric probe has been fulfilled by **L2**. It was employed to three-way detections like naked eye and colorimetric and fluorometric methods to detect the metal ions in a competitive environment. The ligand shows exceptional optical properties and selectivity which can be seen in Figure 3a,b, and the interference effect with other metal ions has been given in the Supporting Information, Figure S5b. The naked eye detection clearly shows a visible color change from yellow to pale orange, and under fluorescent light, a yellow to orange fluorescent color change can be seen. The naked eye detection was further analytically confirmed by both colorimetric and PL studies. We expected that the compound could sense Cu^{2+} as like **L1**. Surprisingly, **L2** shows a selectivity to Cd^{2+}. We also

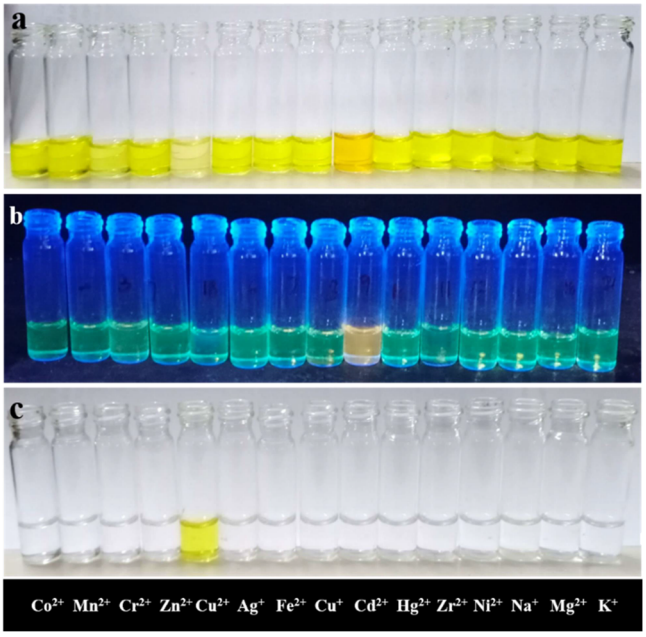

Figure 3. (a) Optical naked eye detection of Cd^{2+} by **L2** under visible light. (b) Visual observation of the color change upon addition of cadmium to **L2** under FL. (c) Perceptible color change upon addition of Cu^{2+} to **L1** and comparative observation with other metal ions.

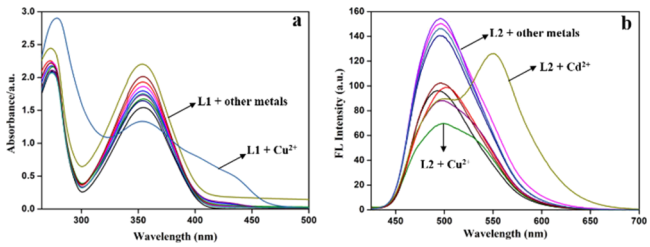

Figure 4. (a) Selectivity of **L1** to Cu^{2+} over other metal ions by UV−vis spectroscopic response and (b) selectivity of **L2** to Cd^{2+} over other competitive metal ions by the PL response.

noticed a noncommendable quench of FL, when Cu^{2+} was added because of its paramagnetic nature. However, the small interference by copper was eliminated by adding a masking agent S^{2-} ion, which forms a stable CuS species. While adding Cd^{2+} there was a commendable weakening of emission intensity at 416 nm, and a new peak was observed at 552 nm. The coordination of cadmium ions increased the planarity of **L2** and therefore increases the conjugation of the probe. Henceforth it exhibits a huge bathochromic shift of 139 nm. There was no significant change in emission when other competitive metal ions were added to **L2** (Figure 4b).

3.3. Sensitivity Studies of L1-Cu^{2+} and L2-Cd^{2+}. To further confirm the formation of ligand−metal complexes, the absorption spectra of probes **L1** and **L2** and PL intensity of **L2** upon addition of Cu^{2+} and Cd^{2+} were investigated. Upon the incremental concentration of Cu^{2+} to **L1**, the 353 nm band gradually decreased. Meanwhile, a new band emerged at 412 nm with the concomitant change from colorless to yellow. A unique isosbestic point at 383 nm indicates the formation of a single metal complex. In accordance with that, there was a linear decrease in absorbance at 353 nm with the increase in concentration of Cu^{2+} in the range of 0−280 μL. Alongside, the absorbance ratio (A_{353}/A_{412}) was also correlated linearly

https://doi.org/10.1021/acsomega.2c05157
ACS Omega 2022, 7, 41361−41369

with the same concentration of Cu^{2+} ion solution (Figure 5a-i–iii). The slope value was obtained from this ratiometric

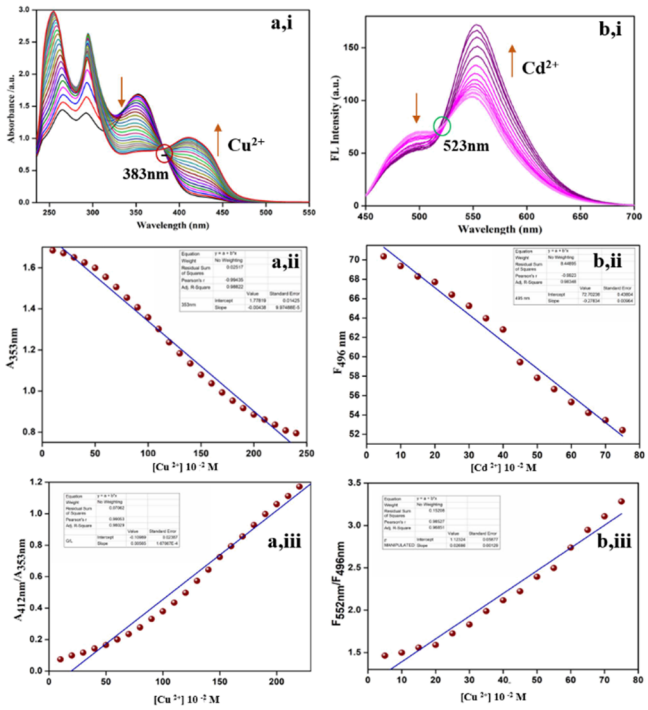

Figure 5. (a,i) Titration response of **L1** in the presence of increasing concentration of Cu^{2+} by UV spectroscopy. (a,ii) Absorbance decreases at 353 nm when Cu^{2+} was added to **L1** gradually. (a,iii) Ratiometric plot A_{412nm}/A_{353nm} of **L1** upon addition of copper ion solution. (b,i) Titration response of **L2** in the presence of increasing concentration of Cd^{2+} by the PL study. (b,ii) FL intensity decreases at 496 nm when Cd^{2+} was added to **L2** gradually. (b,iii) Ratiometric plot F_{552nm}/F_{496nm} of **L2** upon addition of cadmium ion solution.

calibration plot. Thus, limit of detection (LOD) and limit of quantitation (LOQ) values for **L1** were found to be 1.06×10^{-7} M and 3.53×10^{-7} M, respectively.

L2 was one such probe tested for multiple ways of detecting Cd^{2+} ions. Henceforth, it was deployed to naked eye, colorimetric, fluorometric, solid-phase, and real-time sample analyses. All five methods have shown a positive result. The result was outstanding with a striking detection limit in fluorometric detection. Initially, 100 μL of 10^{-2} M Cd^{2+} was added to the 10^{-4} M concentrated solution of **L2**. A visible color change from yellow to pale orange was observed, and further confirmation was done with UV and FL titration. The UV titration shows a significant red shift from 416 to 511 nm (Figure S6). However, the detection limit 1.32×10^{-6} M was quite low when compared with FL studies portraying a striking LOD as 2.25×10^{-9} M and LOQ as 7.50×10^{-10} M. The FL titration shows a ratiometric increment in a new band at 552 nm with a gradual decrease of the band at 496 nm. The calibration plot shows the decrease in FL intensity of L2 upon the addition of Cd^{2+}, and the ratiometric FL intensity (F_{552}/F_{496}) increases gradually with the concentration of metal solution (Figure 5a-i–iii).

3.4. Sensing Mechanism of L1-Cu^{2+} and L2-Cd^{2+}.

Furthermore, the stoichiometric ratio of **L1**:Cu^{2+} and **L2**:Cd^{2+} was found using Job's plot (Figure 6). The absorbance change with different concentrations of **L1** and cupric ions indicated the 2:1 stoichiometric ratio, which was further confirmed by

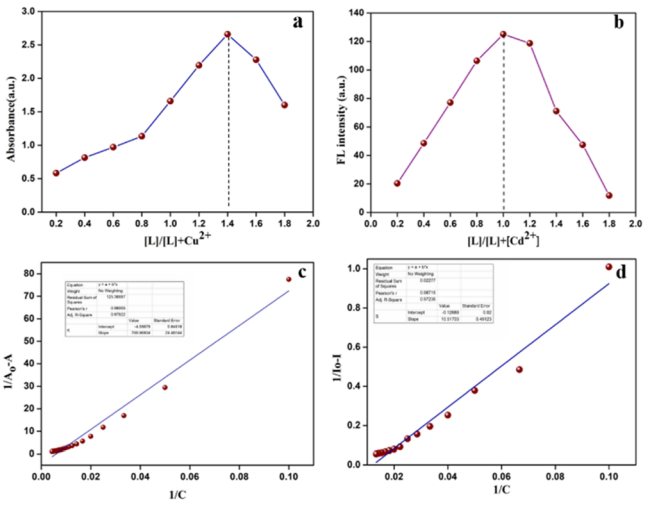

Figure 6. (a) Job's plot and (c) B^H plot of **L1** in the presence of different concentrations of Cu^{2+}; (b) Job's plot and (d) B^H plot of **L2** in the presence of different concentrations of Cd^{2+}.

electrospray ionization-mass spectrometry (ESI-MS). The obtained mass 657.10 matches the calculated mass of 659.12 m/z in +2H mode (Figure S7a). The binding constant was obtained through the Benesi–Hilderband standard formula B_H = intercept/slope from the B_H plot, which shows the binding efficacy of **L1** with Cu^{2+} as 5.93×10^{-3} M^{-1}.

By a similar method, we obtained the stoichiometric ratio of **L2**:Cd^{2+} as 1:1 and binding constant as 1.2×10^{-2} M^{-1}. A solid confirmation was obtained by ESI-MS showing a peak at m/z of 496.93 corresponding to $[\mathbf{L2} + Cd^{2+} - 2H^+]$ (Figure S7b). The final confirmation was obtained through NMR titration spectra in DMSO-d_6. It is well known that there will be a change in electron density of the coordination sites of the ligand when metal binds and thus induces the shift of the nearby proton signals. The scan was done immediately after the addition of Cd^{2+} to the ligand in order to get an appropriate result. The imine proton (H_a) displayed a de-shielding effect of 0.0017 ppm, and the proton adjacent to thiazole nitrogen uplifted to 0.223 ppm (Figure 7a). This situation implied the direct participation of imine and thiazole nitrogen atoms in binding with Cd^{2+} as represented in Scheme 2. Likewise, the NMR titration of **L1** in the presence of various concentrations of Cu^{2+} ions is given in Figure 7b. This figure clearly indicates that there was a complete quenching of the imine CH peak at 8.32 ppm and the CH proton peak adjacent to thiazole nitrogen at 7.72. The outcomes show the direct participation of imine CH and CH protons adjacent to the thiazole nitrogen in metal binding. Thus, the formation of an **L1**-Cu^{2+} complex was confirmed through this titration result.

Thus, the comparison of this research work with the previously reported papers is given in Table 2.[25−27] The results of comparison clearly show that the previously reported thiophene-appended imine-conjugated small molecules do not show any emission spectrum until the metal ion was added. While we achieved in synthesizing fluorescent probe **L2** with a quantum yield of 0.002939, it shows an enhanced emission upon addition of cadmium ions. In **L2**, conjugated thiophene itself acts as a fluorophore, whereas in previously reported molecules the thiophene was just used as a recognizing moiety rather, tuning its photoluminescence properties to make it as fluorometric probe. **L2** is the first of thiophene-appended

https://doi.org/10.1021/acsomega.2c05157
ACS Omega 2022, 7, 41361−41369

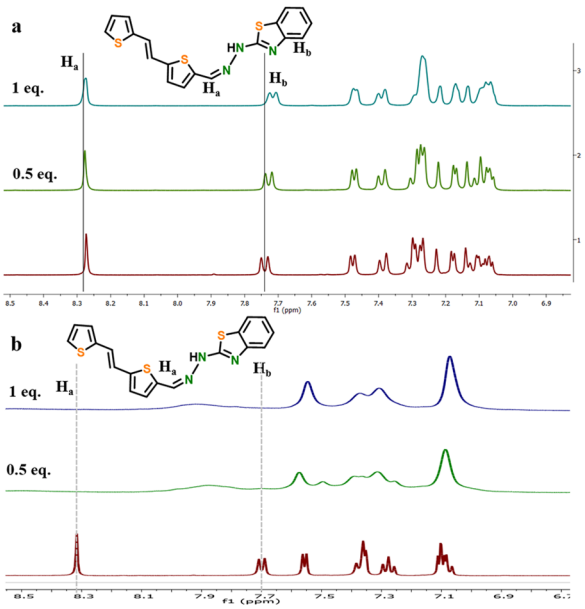

Figure 7. (a) ^{1}H NMR spectra (400 Hz, DMSO-d6) of probe **L1** in the absence and presence of Cu^{2+} ions (0.5, 1 equiv). (b) ^{1}H NMR spectra (400 Hz, DMSO-d6) of probe **L2** in the absence and presence of Cd^{2+} ions (0.5, 1 equiv).

Scheme 2. (a) Schematic Representation of Binding of Cd^{2+} Metal Ions with L2 and (b) Binding Mechanism of Cu^{2+} with L1

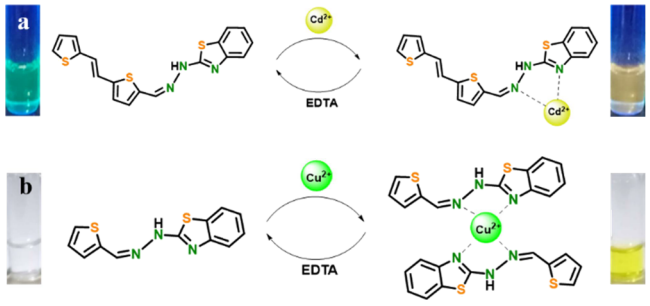

Table 2. Comparison of Efficiency and Uniqueness of L2 with the Previously Reported Thiophene-Appended Conjugated Probe

ref.	fluorophore and recognizing unit	fluorescent mechanism	LOD
13	triphenyl amine and thiophene	turn-on with Cr^{3+}	1.5×10^{-6} M
22	4-diethylaminosalicylaldehyde and thiophene	turn-on with Ln^{3+}	4.48×10^{-8} M
23	anthracene and thiophene	turn-on with Cr^{3+}	0.14×10^{-6} M
24	*o*-aminophenol and thiophene	turn-on with Pb^{2+}, Hg^{2+}, Sn^{2+}	-
this work	thiophene and benzothiazole	fluorescent enhancement with Cd^{2+}	2.25 nM

small molecules to detect cadmium ions with an outstanding LOD of 2.25 nM.

3.5. Reversibility and Response Time Studies of L1-Cu^{2+} and L2-Cd^{2+}. The reusability of the sensing probe is possible when a complexed metal ion was reversed by adding a suitable chelating ligand. This process indulges the reproducibility of the system and can be used multiple times (recycling ability) to detect the desired metal ion. The **L2-Cd^{2+}** complex was reversed by adding EDTA into the system. Figure 8a,b

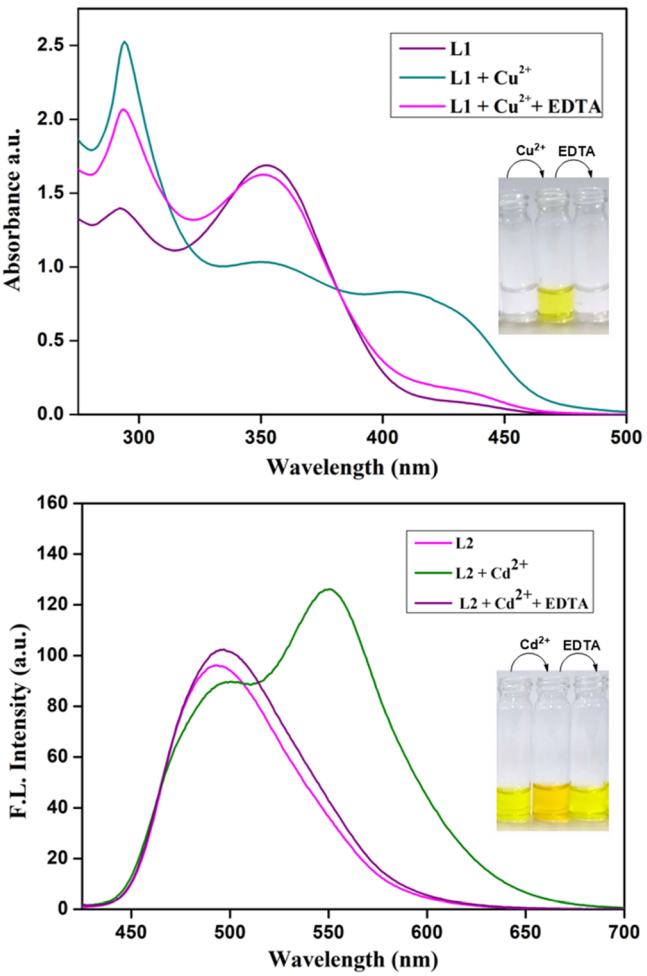

Figure 8. (a) Reversibility of **L1-Cu^{2+}** upon the addition of EDTA. (b) Reversibility of **L2-Cd^{2+}** with EDTA.

demonstrates how the addition of EDTA reduced the FL intensity. The introduced chelating ligand (EDTA) thus captured the cadmium ion to facilitate the renewal of the probe molecule. The process holds good repeatability for six times. Thus, from the above investigation it was clearly noticed that the **L2** can be recycled and reused. Likewise, the repeatability process was also carried out for **L1 + Cu^{2+}** metal complex with five times of repeatability. The outcomes of the reversible experiment display the multiple uses of the probe for sensing applications.

Time of detection of metal ions by the ligands was obtained by recording the change in intensity, and absorbance of the probe for every 2 s. **L2** showcased a vibrant FL change in just 7 s when the FL instrument started to operate. However, according to our timer, the operating procedure took us 5 s to initiate the procedure. Thus, we conclude that the response time of **L2** to the cadmium ion is 12 s (Figure S8).

3.6. DFT Studies and Band Gap Calculation. The electronic states and structural properties of the ligands **L1** and **L2** and the complex **L1-Cu^{2+}** and **L2-Cd^{2+}** were theoretically optimized by DFT calculations. The optimized

https://doi.org/10.1021/acsomega.2c05157
ACS Omega 2022, 7, 41361−41369

structure and molecular orbital diagrams are represented in Figure 9. From the optimized structure, we obtained the bond

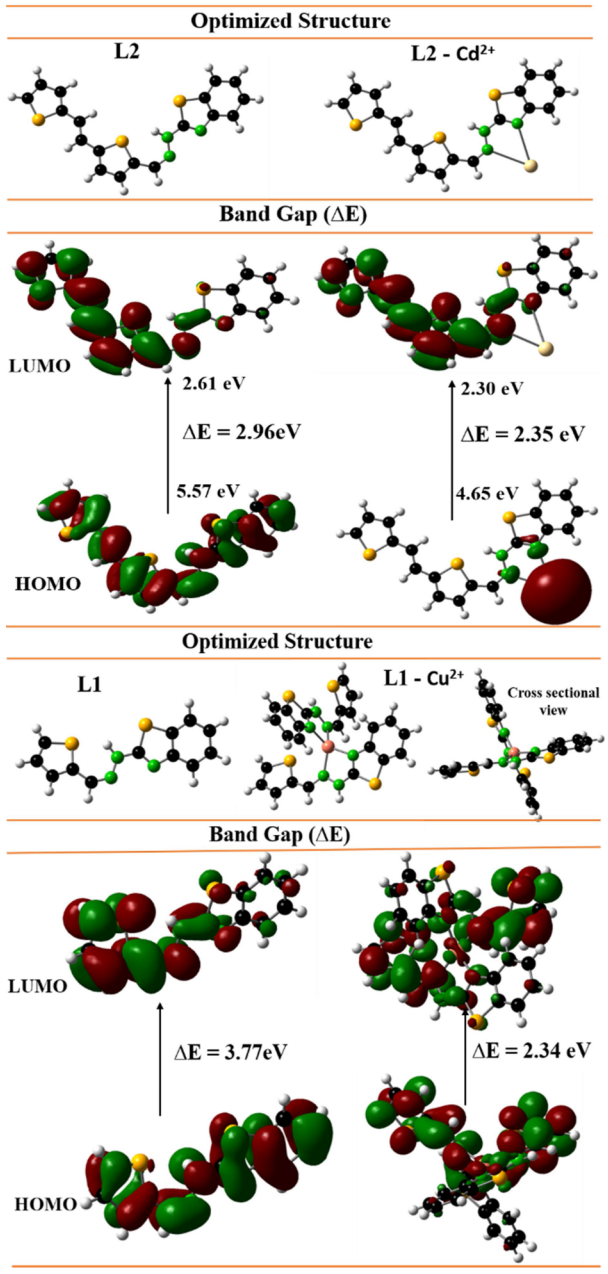

Figure 9. Theoretically optimized structure and frontier molecular orbital (HOMO and LUMO) **L1**, **L1-Cu**$^{2+}$ and **L2**, **L2-Cd**$^{2+}$ obtained by DFT-B3LYP and 6-31G(d)/LANL2DZ program.

length CH═N−Cd and C═N−Cd as 3.294 and 3.343 Å, respectively, in the **L2-Cd**$^{2+}$ complex. The stability of the metal ligand coordination was further confirmed with the calculated interaction energy value. This indicates the greater stability of the metal ligand complex. The experimental optical band gap obtained by Tauc's plots of $(\alpha h\nu)^2$ versus photoenergy $(h\nu)$ was found to be less than the theoretically obtained band gap using the B3LYP/6-31+G** level in the gas phase. The theoretically calculated bandgap of **L2** and **L2-Cd**$^{2+}$ was found to be 2.96 and 2.35 eV, respectively, whereas through Tauc's plot we determined the band gap of **L2** as 2.31 eV and for **L2-Cd**$^{2+}$ complex as 2.24 eV. The decreased band gap obtained by experimental data than DFT calculations is due to the consideration of variable factors including the experimental procedure, analysis environment, and consideration of the overall molecule instead of one single moiety.

In free **L2**, electron density of the highest occupied molecular orbital (HOMO) was completely distributed over the entire molecule, and the electron density of the lowest unoccupied molecular orbital (LUMO) was centered in conjugated thiophene. Thus, it depicts the ICT from the HOMO to LUMO. In the **L2-Cd**$^{2+}$ complex, it can be concluded easily that electron density of the HOMO centered in the metal ion and the electron density of the LUMO centered in conjugated thiophene, which probably nullified the ICT between thiophene and benzothiazole. Thus enhanced metal ligand charge transfer (MLCT) between cadmium and conjugated thiophene was observed. This MLCT results in $n-\pi^*$ transition between the ligand **L2** and cadmium ion.

The band gap of **L1** is much greater than that of **L2**; this was probably due to the nonlinearity of **L1** due to limited π conjugation. However, the band gap of **L1-Cu**$^{2+}$ is much less than that of **L2-Cd**$^{2+}$ complex because an extended conjugation results in an increase in planarity of the metal complex. This result was also confirmed by a decreased band gap of 2.01 eV when compared to its respective ligand **L1** and less even in comparison with **L2-Cd**$^{2+}$ (2.24 eV). Both in theoretical and practical observations the band gap of **L1-Cu**$^{2+}$ was found to be less than that of **L2-Cd**$^{2+}$ (Figure 10).

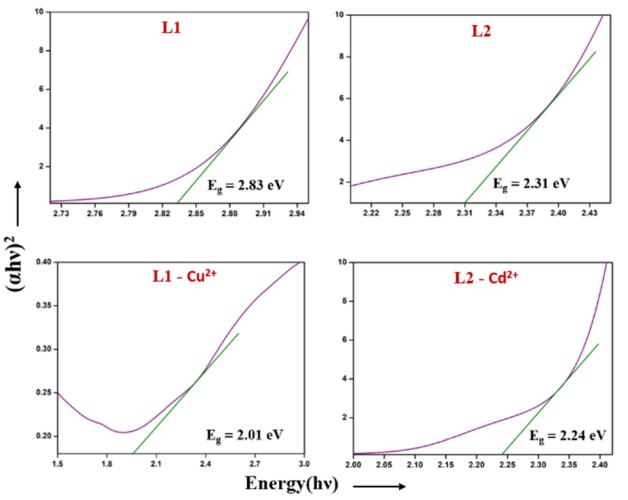

Figure 10. Tauc's plots of $(\alpha h\nu)^2$ versus photon energy $(h\nu)$ of **L1**, **L1-Cu**$^{2+}$, **L2**, and **L2-Cd**$^{2+}$.

3.7. Test Strip, Solid-State Detection, and Real-Sample Analysis. The qualitative analysis was carried out by preparing a test strip coated with the ligands **L1** and **L2**. When the respective metal ion solution of calculated amount was added onto the strip, a color change was observed. For the **L1** strip, it changed from colorless to bright yellow, and for the **L2** strip, the color changes from yellow to orange. The vibrant color changes were seen, which is given in Figure 11d,e. In addition to the above-mentioned test, the **L1**- and **L2**-coated silica gel was exposed to Cu^{2+} and Cd^{2+} solution. The ligand solutions of **L1** and **L2** were mixed separately with silica gel and dried in a hot air oven. The colors of **L1**- and **L2**-coated silica gel were white and yellow, respectively. Then the calculated amount of metal solutions was added to the respective ligand-coated silica gel and then dried.

https://doi.org/10.1021/acsomega.2c05157
ACS Omega 2022, 7, 41361−41369

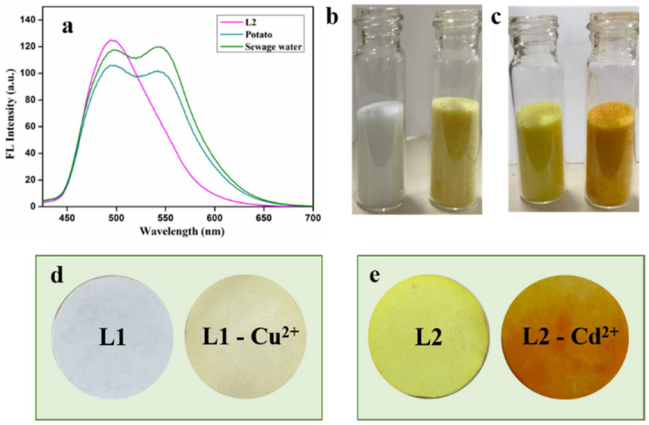

Figure 11. (a) FL response of **L2** upon addition of Cd^{2+} purged real time, samples potato extract and sewage water, (b) solid-phase detection of Cu^{2+} using **L1** in silica gel, (c) solid-phase detection of Cd^{2+} using **L2** in silica gel, (d) color change after the addition Cu^{2+} to **L1**-loaded test strip, and (e) color change after the addition Cd^{2+} to the **L2**-loaded test strip.

We observed a significant color change of **L1** from white to yellow upon the addition of Cu^{2+} and **L2** from yellow to orange upon addition of Cd^{2+}.

The quantitative practical applicability of the synthesized probe **L2** was tested by detecting the cadmium ion in the sewage water and the potato extract. The details of extraction and filtration of the samples are already mentioned in the Experimental Section. The change of intensity at 552 nm can be seen in Figure 11a. The samples were tested in potato extract and sewage water for the detection of cadmium ions. The recovery of spiked-up Cd^{2+} in potato was found to be 98 percentage, whereas in sewage water it was 96 percentage. This proves that the probe can be used for detecting the sample from the variable environment after making a necessary adjustment in the pH value.

3.8. FL Life Time. Life time of FL can be measured by recording the intensity of FL versus time of decay (Figure S9). For the experimental procedure, a silicon colloid was taken as an internal standard or prompt. The calibration had been obtained with a chi square value of 1.5 for a proximal determination of standard deviation of the curve. The life time of FL of **L2** was 58.3 ps, whereas the time period for the complete decay of metal complex **L2-Cd^{2+}** was 0.147 ns, which was found to be much higher than that of **L2**. This was probably due to the stability of the metal complex with enhanced FL at 552 nm in FL observation.

4. CONCLUSIONS AND FUTURE PERSPECTIVE

Herein, we report a comparison of ratiometric sensing application of **L1** and **L2**. A novel FL ratiometric sensing probe **L2** exhibits a pronounced selectivity and sensitivity in detecting cadmium ions. Despite **L1** having an outstanding selectivity for the copper, the detection limit was found to be lower than that of **L2**. The emission spectrum is also lacking. However, **L2** shows an ease for PL ratiometric detection of Cd^{2+} with a striking LOD of 2.25 nM. It is noteworthy that the limit was way less than the permitted level of cadmium in real-time samples. Additionally, it was proven to be effective in detecting Cd^{2+} in all conceivable contexts like naked eye, colorimetric, fluorometric, solid state, strip-based, and in real-time samples. Among the top, the recovery of the spiked-up cadmium level 99% in sewage water and 98% in potato extract shows its application in the detection of metal ions in the environment. Thus, it marked a way for developing a portable sensor in future, and the decreased band gap makes it a potential probe for developing an optical device.

■ ASSOCIATED CONTENT

Supporting Information

The Supporting Information is available free of charge at https://pubs.acs.org/doi/10.1021/acsomega.2c05157.

1H-NMR, 13C-NMR, HRMS, UV−vis spectra in the liquid phase and solid phase, UV titration, B−H plot, UV calibration curve, interference bar chart time response curve, FL lifetime graph, and quantum yield calculation (PDF)

■ AUTHOR INFORMATION

Corresponding Author

Subramanian Karpagam − *Department of Chemistry, School of Advanced Sciences, Vellore Institute of Technology, Vellore, Tamil Nadu 632014, India;* orcid.org/0000-0002-7498-2516; Phone: 91-416-2202334; Email: skarpagam80@yahoo.com; Fax: 91-416-2243092

Author

Palani Purushothaman − *Department of Chemistry, School of Advanced Sciences, Vellore Institute of Technology, Vellore, Tamil Nadu 632014, India*

Complete contact information is available at: https://pubs.acs.org/10.1021/acsomega.2c05157

Author Contributions

The manuscript was written through contributions of all authors.

Notes

The authors declare no competing financial interest.

■ ACKNOWLEDGMENTS

The author gratefully acknowledges VIT University for providing "VIT SEED GRANT" to support this work and providing the instrumental affairs.

■ REFERENCES

(1) Palani, P.; Karpagam, S. Conjugated polymers-a versatile platform for various photophysical, electrochemical and biomedical applications: A comprehensive review. *New J. Chem.* **2021**, *45*, 19182−19209.

(2) Umabharathi, P. S.; Karpagam, S. Thiazole-Formulated Azomethine Compound for Three-Way Detection of Mercury Ions in Aqueous Media and Application in Living Cells. *ACS Omega* **2022**, *7*, 24638−24645.

(3) Zehra, S.; Khan, R. A.; Alsalme, A.; Tabassum, S. Coumarin Derived "Turn on" Fluorescent Sensor for Selective Detection of Cadmium (II) Ion: Spectroscopic Studies and Validation of Sensing Mechanism by DFT Calculations. *J. Fluoresc.* **2019**, *29*, 1029−1037.

(4) Li, W.; Jiang, C.; Sheng, L.; Wang, F.; Zhang, Z.; Wei, T.; Chen, Y.; Qiang, J.; Ziyi, Y.; Chen, X. A hydrogel microsphere-based sensor for dual and highly selective detection of Al3+ and Hg2+. *Sens. Actuators, B* **2020**, *321*, No. 128490.

(5) Chen, T.; Wei, T.; Zhang, Z.; Chen, Y.; Qiang, J.; Wang, F.; Chen, X. Highly sensitive and selective ESIPT-based fluorescent probes for detection of Pd^{2+} with large Stocks shifts. *Dyes Pigm.* **2017**, *140*, 392−398.

(6) Rasmussen, S. C.; Evenson, S. J.; McCausland, C. B. Fluorescent thiophene-based materials and their outlook for emissive applications. *Chem. Commun.* **2015**, *51*, 4528−4543.
(7) Lindgren, E. B.; Yoneda, J. D.; Leal, K. Z.; Nogueira, A. F.; Vasconcelos, T. R. A.; Wardell, J. L.; Solange, M. S. V.; Wardell. Structures of hydrazones, (*E*)-2-(1,3-benzothiazolyl)-NHNCHAr, [Ar = 4-(pyridin-2-yl)phenyl, pyrrol-2-yl, thien-2-yl and furan-2-yl]: Difference in conformations and intermolecular hydrogen bonding. *J. Mol. Struct.* **2013**, *1036*, 19−27.
(8) Vijay, N.; Balamurugan, G.; Venkatesan, P.; Wu, S. P.; Velmathi, S. A triple action chemosensor for Cu2+ by chromogenic, Cr3+ by fluorogenic and CN- by relay recognition methods with bio-imaging of HeLa cells. *Photochem. Photobiol. Sci.* **2017**, *16*, 1441−1448.
(9) İnal, E. K. A Fluorescent Chemosensor Based on Schiff Base for the Determination of Zn2+, Cd2+and Hg2+. *J. Fluoresc.* **2020**, *30*, 891−900.
(10) Hayat, M. T.; Nauman, M.; Nazir, N.; Ali, S.; Bangash, N. *Environmental Hazards of Cadmium: Past, Present, and Future*; Elsevier Inc., 2018
(11) Hussain, A.; Murtaza, G.; Ghafoor, A.; Basra, S. M. A.; Qadir, M.; Sabir, M. Cadmium contamination of soils and crops by long term use of raw effluent, ground and canal waters in agricultural lands. *Int. J. Agric. Biol.* **2010**, *12*, 851−856.
(12) Aydin, Z.; Keleş, M. Colorimetric cadmium ion detection in aqueous solutions by newly synthesized Schiff bases. *Turk. J. Chem.* **2020**, *44*, 791−804.
(13) Nath, S.; Bhattacharya, B.; Sarkar, U.; Singh, T. S. Photophysical investigation of a donor-acceptor based Schiff base in solvents of varying polarities. *J. Mol. Struct.* **2022**, *1255*, No. 132435.
(14) Dey, S.; Purkait, R.; Pal, K.; Jana, K.; Sinha, C. Aggregation-Induced Emission-Active Hydrazide-Based Probe: Selective Sensing of Al 3+, HF 2- , and Nitro Explosives. *ACS Omega* **2019**, *4*, 8451−8464.
(15) Li, J.; Chen, Y.; Chen, T.; Qiang, J.; Zhang, Z.; Wei, T.; Zhang, W.; Wang, F.; Chen, X. A benzothiazole-based fluorescent probe for efficient detection and discrimination of Zn^{2+} and Cd^{2+}, using cysteine as an auxiliary reagent. *Sens. Actuators, B* **2018**, *268*, 446−455.
(16) Kolcu, F.; Erdener, D.; Kaya, İ. A Schiff base based on triphenylamine and thiophene moieties as a fluorescent sensor for Cr (III) ions: Synthesis, characterization and fluorescent applications. *Inorg. Chim. Acta* **2020**, *509*, No. 119676.
(17) Musikavanhu, B.; Muthusamy, S.; Zhu, D.; Xue, Z.; Qian, Y.; Chiyumba, C. N.; Mack, J.; Nyokon, T.; Wang, S.; Zhao, L. A simple quinoline-thiophene Schiff base turn-off chemosensor for Hg2+ detection: spectroscopy, sensing properties and applications. *Spectrochim. Acta, Part A* **2022**, *264*, No. 120338.
(18) Wang, J. H.; Liu, Y. M.; Bin, C. J.; Wang, Y.; Wang, H.; Shuang, S. M. A phenazine-imidazole based ratiometric fluorescent probe for Cd2+ ions and its application in in vivo imaging. *Anal. Methods* **2022**, *14*, 1462−1470.
(19) Vinoth Kumar, G. G.; Kannan, R. S.; Chung-Kuang Yang, T.; Rajesh, J.; Sivaraman, G. An efficient "ratiometric" fluorescent chemosensor for the selective detection of Hg 2+ ions based on phosphonates: Its live cell imaging and molecular keypad lock applications. *Anal. Methods* **2019**, *11*, 901−916.
(20) Viswanathan, T.; Palanisami, N. Ferrocene-appended boronated ester: effect of cyanovinylene group on the nonlinear optical properties and colorimetric detection of fluoride ion. *New J. Chem.* **2021**, *45*, 12509−12518.
(21) Baerends, E. J.; Gritsenko, O. V.; Van Meer, R. The Kohn-Sham gap, the fundamental gap and the optical gap: The physical meaning of occupied and virtual Kohn-Sham orbital energies. *Phys. Chem. Chem. Phys.* **2013**, *15*, 16408−16425.
(22) Parvarinezhad, S.; Salehi, M. Synthesis, characterization, anti-proliferative activity and chemistry computation of DFT theoretical methods of hydrazine-based Schiff bases derived from methyl acetoacetate and α-hydroxyacetophenone. *J. Mol. Struct.* **2021**, *1225*, No. 129086.
(23) Mahesh, K.; Karpagam, S. Synthesis and Optoelectronic Properties of Thiophene Donor and Thiazole Acceptor Based Blue Fluorescent Conjugated Oligomers. *J. Fluoresc.* **2016**, *26*, 1457−1466.
(24) Lasitha, P.; Dasgupta, S.; Naresh, P. G. Unraveling the Origin of Differentiable 'Turn-On' Fluorescence Sensing of Zn2+ and Cd2+ Ions with Squaramides. *ChemPhysChem* **2020**, *21*, 1564−1570.
(25) Xing, Y.; Liu, Z.; Yuankang, X.; WanG, H.; Li, L.; Li, B.; Yang, X.; Peia, M.; Zhang, G. Double Schiff base from thiophene-2,5-dicarboxylic acid as an "off-on-off" fluorescence sensor for the sequential detection of In^{3+} and PPi. *New J. Chem.* **2020**, *44*, 13875−13881.
(26) Karakuş, E. An anthracene based fluorescent probe for the selective and sensitive detection of Chromium (III) ions in an aqueous medium and its practical application. *Turk. J. Chem.* **2020**, *44*, 941−949.
(27) Udhayakumari, D.; Suganya, S.; Velmathi, S.; MubarakAli, D. Naked eye sensing of toxic metal ions in aqueous medium using thiophene-based ligands and its application in living cells. *J. Mol. Recognit.* **2014**, *27*, 151−159.

https://doi.org/10.1021/acsomega.2c05157
ACS Omega 2022, 7, 41361−41369